Penetrable-square-well fluids: Analytical study and Monte Carlo simulations

Riccardo Fantoni,[1,a)] Achille Giacometti,[1,b)] Alexandr Malijevský,[2,c)] and Andrés Santos[3,d)]

[1]*Dipartimento di Chimica Fisica, Università di Venezia, Calle Larga S. Marta DD2137,
I-30123 Venezia, Italy*
[2]*E. Hála Laboratory of Thermodynamics, Academy of Science of the Czech Republic,
Prague 6, Czech Republic and Department of Chemical Engineering, Institute of Theoretical Physics,
Imperial College London, South Kensington Campus, London SW7 2BZ, United Kingdom*
[3]*Departamento de Física, Universidad de Extremadura, Badajoz E-06071, Spain*

We study structural and thermophysical properties of a one-dimensional classical fluid made of penetrable spheres interacting via an attractive square-well potential. Penetrability of the spheres is enforced by reducing from infinite to finite the repulsive energy barrier in the pair potentials As a consequence, an exact analytical solution is lacking even in one dimension. Building upon previous exact analytical work in the low-density limit [A. Santos, R. Fantoni, and A. Giacometti, Phys. Rev. E **77**, 051206 (2008)], we propose an approximate theory valid at any density and in the low-penetrable regime. By comparison with specialized Monte Carlo simulations and integral equation theories, we assess the regime of validity of the theory. We investigate the degree of inconsistency among the various routes to thermodynamics and explore the possibility of a fluid-fluid transition. Finally we locate the dependence of the Fisher–Widom line on the degree of penetrability. Our results constitute the first systematic study of penetrable spheres with attractions as a prototype model for soft systems. © *2009 American Institute of Physics*.
[doi:10.1063/1.3236515]

I. INTRODUCTION

Hard spheres constitute a paradigmatic system for many simple and complex fluids. Steric stabilized colloids, for instance, are suspensions made of colloidal particles coated by short linear polymers suspended in a microscopic solvent fluid. For sufficiently high temperature and/or in the presence of a good solvent, those dressed colloids effectively interact as hard spheres.[1]

On the other hand, a number of soft colloidal systems is always penetrable at least to a certain extent.[2] Notable examples include for instance star-shaped[3] or branched-shaped[4] polymers where each macromolecule can be roughly regarded as a sphere of a given radius (the radius of gyration), but two particles can clearly interpenetrate to a substantially smaller distance.

A necessary (but not sufficient) condition for a one-dimensional fluid to be a *nearest-neighbor* fluid is to be a hard-core fluid, i.e., a fluid made of particles which cannot penetrate one another due to the existence of an infinite repulsive potential barrier in the pair potential $\phi(r)$. Nearest-neighbor fluids admit an analytical exact statistical-mechanical solution:[5] The partition function, equation of state, and correlation functions of any order can be calculated analytically from the knowledge of the pair potential. This is no longer the case for non-neighbor fluids.[6]

Penetrable spheres (PSs)[7,8] can be reckoned as the simplest representation of soft colloids where the range of penetrability can be tuned from zero (hard spheres) to infinity (ideal gas). Both limits are amenable to an exact analytical treatment, but the intermediate case is not.

When an attractive, short-range, square well (SW) is added to PS, one obtains the so-called penetrable-SW (PSW) fluid.[10] On one hand, this enriches the model so that it can also account for short-range attractive interactions which are ubiquitous in such systems. On the other hand, it also complicates the treatment due to possible Ruelle instabilities associated with the lack of a well defined thermodynamic limit.[11,12] As the width of the well vanishes with a constant area under the well, the PSW model reduces to what we denote[10] as the sticky-penetrable-sphere (SPS) model. This model was found to be thermodynamically unstable[10] due to the divergence of the fourth virial coefficient. In fact, SPS model violates the (sufficient) condition for stability (see Appendix A in Ref. 10).

We emphasize that various classes of penetrable systems appeared in the literature with rather different meanings. The Widom–Rowlinson model of nonadditive hard-sphere mixtures,[13] for instance, is not associated with a well defined pair potential as in the case of the present study. Likewise, the Rikvold–Stell–Torquato "permeable sphere" model[14,15] is defined through a condition on correlation function which is not equivalent to a constant repulsive potential inside the core region. On the contrary, our PSW model belongs to the same class of bounded potentials as the Gaussian-core mod-

---

a)Electronic mail: rfantoni@unive.it.
b)Electronic mail: achille@unive.it.
c)Electronic mail: amail@post.cz.
d)Electronic mail: andres@unex.es. URL: http://www.unex.es/fisteor/andres/

els originally proposed by Stillinger *et al.*[16] in the late 1970s and exploited more recently by Likos *et al.*,[8] Lang *et al.*,[9] and Louis *et al.*[17]

In a previous paper,[10] we introduced the PSW fluid model and discussed the conditions under which the model is Ruelle stable. In addition, we also derived an exact low-density expansion up to second order in the radial pair distribution function (corresponding to the fourth order in the virial coefficient) which was shown to compete with standard integral equation approximations such as Percus–Yevick (PY) and hypernetted chain (HNC) over a wide region of the density-temperature phase diagram. These exact results, however, fail to reproduce the correct behavior when the concentration is large, due to their low-density character.

The aim of the present paper is to extend the analysis to these more demanding conditions, by using an approximation already successfully exploited in the PS case. In this case it has been argued[7] that the exact analytical solution stemming from corresponding hard-sphere particles can be efficiently exploited to implement a low-penetrability approximate solution (called LTA in Ref. 7). The basic idea behind the method is that for sufficiently low penetrability, the functional form of the equations derived in the impenetrable case can be smoothly adapted to the penetrable case by "healing" a few crucial aspects of the original solution. Building on this idea, we here show that this methodology can also be applied to the PSW case by starting from the corresponding impenetrable counterpart (i.e., the SW potential).

We discuss the soundness of this approximation in various ways: First by comparing the low-penetrability approximation (LPA) low-density results against the exact low-density expansion which was computed in Ref. 10 and, second, by comparing with specialized Monte Carlo (MC) simulations and standard integral equations (notably PY and HNC). We show how LPA properly describes a significant part of the phase diagram with a performance comparable with integral equations at a semianalytical level.

The introduction of an attractive part in the PS potential opens the route to some interesting questions that we also address in the present paper. First of all, we question the existence of a fluid-fluid phase separation in addition to the fluid-solid transition, by limiting our analysis within the range of applicability of LPA, that is, we avoid densities so high that a substantial interpenetration among particles is expected.

Within the same LPA, we also investigate modifications on the Fisher–Widom (FW) line, marking the transition from oscillatory to exponential decay regimes for correlation functions, that is known to exist even in the SW one-dimensional fluid.[18] We find an increase in the exponential decay region and we address the physical motivations behind this.

The structure of the paper is as follows. We define the PSW model in Sec. II. In Sec. III we briefly recall the well known general scheme allowing for the exact analytical solution of the class of nearest-neighbor one-dimensional fluids. We then construct the LPA in Sec. IV and show how this reduces to its counterpart within the PS limit[7] and assess its performance in comparison with known exact results within
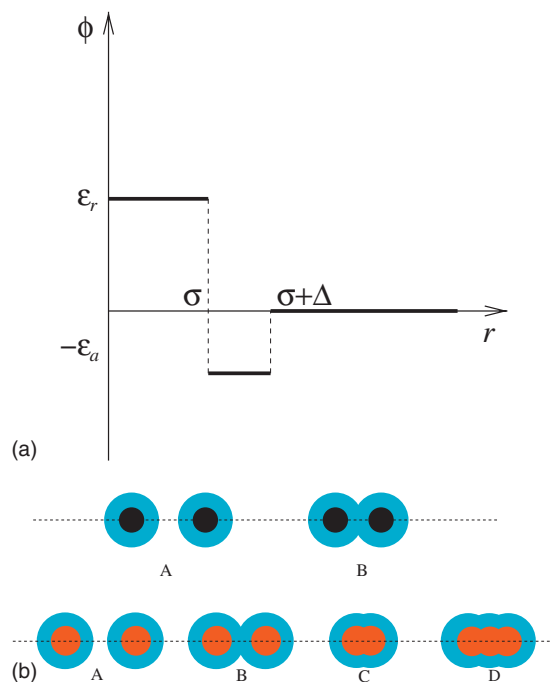

FIG. 1. The PSW potential (top panel). The middle and bottom panels sketch the different behaviors of the SW and PSW models, respectively. In the SW case there exists a hard core (black inner sphere) and an interaction range (light blue outer sphere) so two spheres on a line can either noninteract (A) or attract each other as the corresponding interaction spheres overlap (B). As a consequence, different spheres cannot interchange positions on a one-dimensional line and the problem is analytically solvable. In the PSW the core is soft (red inner sphere) and hence we can have in addition to configurations (A) and (B) identical to the SW case, also the case where the internal cores overlap such as (C) and (D). Different spheres can then interchange position and the problem is a many-body one.

the low-density limit.[10] Sections V and VI contain a discussion on the FW line and on the routes to thermodynamics, as predicted by the LPA, respectively. The regions in the density-temperature diagram where the LPA is only slightly thermodynamically inconsistent (and thus expected to be reliable) are discussed in Sec. VII, where also an improved version of the approximation is proposed. Section VIII includes a very brief description on the numerical methods (MC simulations and integral equations) discussed in the present model. These numerical results are presented and compared with LPA theory in Sec. IX. The paper ends with some concluding remarks in Sec. X.

II. THE PENETRABLE-SQUARE-WELL MODEL

The PSW fluid is defined through the following pair potential[10] (see Fig. 1, top panel),

$$\phi(r) = \begin{cases} \epsilon_r, & r < \sigma, \\ -\epsilon_a, & \sigma < r < \sigma + \Delta, \\ 0, & r > \sigma + \Delta, \end{cases} \quad (1)$$

where ϵ_r and ϵ_a are two positive constants accounting for the repulsive and attractive parts of the potential, respectively. The corresponding Mayer function $f(r) = e^{-\beta\phi(r)} - 1$ (where $\beta = 1/k_B T$ is the inverse temperature parameter) reads

$$f(r) = \gamma_r f_{\text{HS}}(r) + \gamma_a[\Theta(r - \sigma) - \Theta(r - \sigma - \Delta)], \qquad (2)$$

where $\gamma_r = 1 - e^{-\beta\epsilon_r}$ is the parameter measuring the degree of penetrability varying between 0 (free penetrability) and 1 (impenetrability) and $\gamma_a = e^{\beta\epsilon_a} - 1 > 0$ plays a similar role for the attractive part. Here $f_{\text{HS}}(r) = \Theta(r - \sigma) - 1$ is the Mayer function for the hard-sphere model which can then be recovered in the limit $\gamma_r \to 1$ and either $\gamma_a \to 0$ or $\Delta \to 0$. $\Theta(r)$ is the usual step function equal to 1 for $r > 0$ and 0 otherwise. It also proves convenient to introduce the ratio $\gamma = \gamma_a / \gamma_r$, which is a measure of the relative depth of the attractive well.

The above potential reduces to the corresponding PS and SW potentials in the limits $\epsilon_a \to 0$ (or $\Delta \to 0$) and $\epsilon_r \to \infty$, respectively. Other interesting limiting cases have already been detailed in Ref. 10.

Consider a SW fluid in one dimension: different particles can be assigned an increasing coordinate on the axis line and the only possible configurations are those indicated with (A) or (B) in Fig. 1 (middle panel), where either the centers of two different spheres are separated a distance greater than the attractive SW range and behave as hard spheres (A) or they are sufficiently close to attract each other (B). PSW spheres, on the other hand, can interpenetrate with some energy cost so they also display configurations such as, for instance, (C) or (D) in Fig. 1 (bottom panel). PSW fluids are then effectively a many-body problem and, as such, not amenable to an analytical solution. In the present paper, our analysis will be limited to the case $\epsilon_r > 2\epsilon_a$ where a well defined thermodynamic limit is ensured.[10]

III. GENERAL RECIPE FOR NEAREST-NEIGHBOR INTERACTIONS

In this section we provide a synopsis of the main steps required by the analytical solution of any nearest-neighbor fluid.[5,19,20] This will be used in the next section to introduce a motivated approximate solution in a particular limit.

- From the Boltzmann factor $e^{-\beta\phi(r)}$ compute its Laplace transform

$$\tilde{\Omega}(s) = \int_0^\infty dr e^{-sr} e^{-\beta\phi(r)}. \qquad (3)$$

- The equation of state is given by

$$\beta p = \frac{\xi}{\sigma}, \qquad (4)$$

where p is the pressure and the parameter ξ is the solution of the equation,

$$\rho = -\frac{\tilde{\Omega}(\xi/\sigma)}{\tilde{\Omega}'(\xi/\sigma)}, \qquad (5)$$

where ρ is the density and $\tilde{\Omega}'(s) = \partial\tilde{\Omega}(s)/\partial s$. This provides all thermodynamics.

- The radial distribution function (RDF) can be obtained from

$$\tilde{G}(s) = \frac{1}{\rho} \frac{\tilde{\Omega}(s + \xi/\sigma)}{\tilde{\Omega}(\xi/\sigma) - \tilde{\Omega}(s + \xi/\sigma)}, \qquad (6)$$

which is the Laplace transform of the RDF $g(r)$.

This is sufficient to compute both thermodynamics and structural properties of any one-dimensional system with nearest-neighbor interactions.

At odds to this class of problems, PSs do not possess any analytical solution even in one dimension. This is because it is not possible to convolute appropriate Laplace transform along a one-dimensional axis, which is the essential feature rendering the short-range one-dimensional models solvable. In turn this is due to the existence of multiple "blobs" formed by interpenetrating spheres so that it is no longer possible to "order" them along a line in such a way that they do not cross each other, a key point to the existence of the analytical solution (see Fig. 1, middle panel). Because of this, we now turn our attention to a motivated approximation which amounts to assume a slight decrease from an infinite repulsive barrier, an approximation which will be denoted as low penetrability.

IV. THE LOW-PENETRABILITY APPROXIMATION

A. Construction of the approximation

In Ref. 10 we followed the philosophy of considering a low-density expansion to provide exact analytical results valid up to second order in the RDF $g(r)$ and up to fourth order in the virial expansion. This is a very useful exact limit case to test approximate theories and numerical simulations, but it has the considerable disadvantage of being limited to very low densities. We now consider a different approach where density can in principle be arbitrarily large but we assume low penetrability among different spheres, patterned after a similar idea already used in the PS case.[7]

For notational simplicity, in the following, lengths will be measured in units of σ (so that $\sigma = 1$) and we introduce $\lambda = 1 + \Delta/\sigma$ as a dimensionless measure of the external well boundary. The Laplace transform of the Boltzmann factor $e^{\beta\phi(r)}$ for the PSW model is

$$\tilde{\Omega}(s) = \frac{1 - \gamma_r}{s} + \frac{\gamma_r}{s}[(1 + \gamma)e^{-s} - \gamma e^{-\lambda s}]. \qquad (7)$$

The PSW fluid is not a nearest-neighbor fluid, as remarked, but it reduces to the nearest-neighbor SW fluid as $\gamma_r \to 1$ (and $\Delta < 1$). In this limit, it is natural to use the recipe given in Sec. III for the SW fluid to derive an approximate equation of state and an approximate $g(r)$ from Eqs. (4)–(6), respectively. This, however, must be exercised with care as important general properties of any model, such as, for instance, the continuity of the cavity function $y(r) = g(r)e^{\beta\phi(r)}$, are typically lost by this brute force procedure. The driving idea behind this simple LPA is then to keep the general features of the original SW solution and enforce some specific modifications guided by the accounting of increasingly important constraints.[21]

Our LPA implementation amounts to replacing Eq. (6) with

$$\widetilde{G}(s) = \frac{1}{\rho} \frac{\widetilde{\Omega}(s+\zeta)}{\widetilde{\Omega}_0(\zeta) - \widetilde{\Omega}_0(s+\zeta)}, \tag{8}$$

where $\widetilde{\Omega}_0(s)$ is (formally) the Laplace transform of the Boltzmann factor of the SW model, which can be obtained from $\widetilde{\Omega}(s)$ by discarding the first term on the right-hand side of Eq. (7), i.e.,

$$\widetilde{\Omega}_0(s) = \frac{\gamma_r}{s}[(1+\gamma)e^{-s} - \gamma e^{-\lambda s}]. \tag{9}$$

This simple choice can be shown to be fully equivalent to keeping Eq. (6) but with a replacement $e^{-s} \to e^{-(s-a)}$ in Eq. (7), where the free parameter a is fixed by the continuity condition of the cavity function $y(r)$ at the hard-core discontinuity $r=1$. This is known to be the most important feature to obtain a correct representation in integral equation theories of SW fluids, both from the analytical and the numerical viewpoints.[22–24]

We note that, unlike the SW counterpart, $\zeta \neq \beta p$. It is a transcendental function of β and ρ, which can be obtained by ensuring the correct behavior of $g(r) \to 1$ as $r \to \infty$, or, equivalently, $s\widetilde{G}(s) \to 1$ as $s \to 0$. From Eq. (8), this gives

$$\rho = -\frac{\widetilde{\Omega}(\zeta)}{\widetilde{\Omega}_0'(\zeta)} = \zeta \frac{h+1-q}{1-q+(1-\lambda q)\zeta}, \tag{10}$$

where in the second equality we introduced the following quantities:

$$q = \frac{\gamma}{1+\gamma}e^{-\zeta\Delta}, \tag{11}$$

$$h = \frac{1-\gamma_r}{\gamma_r(1+\gamma)}e^{\zeta}. \tag{12}$$

For given values of the potential parameters (Δ, ϵ_r, and ϵ_a) and for given values of the inverse temperature β and the auxiliary parameter ζ, the quantities q and h are obtained from Eqs. (11) and (12) and inserted into Eq. (10) to determine the density ρ. The impenetrable SW potential corresponds to the limit $h \to 0$.

In order to compute the RDF $g(r)$ we first compute explicitly $\widetilde{G}(s)$ from Eqs. (6) and (7),

$$\widetilde{G}(s) = \frac{1}{\rho} \frac{h+e^{-s}(1-qe^{-s\Delta})}{(1-q)(1+s/\zeta) - e^{-s}(1-qe^{-s\Delta})}. \tag{13}$$

Upon expanding the denominator in Eq. (13) in powers of $(1-qe^{-s\Delta})(1+s/\zeta)$, and inverting the Laplace transform term by term, one gets

$$\rho g(r) = \frac{h\zeta}{1-q}e^{-\zeta r} + \sum_{n=1}^{\infty}\sum_{k=0}^{n}\binom{n}{k}(-q)^k \psi_n(r-n-k\Delta)$$
$$\times \Theta(r-n-k\Delta), \tag{14}$$

where

$$\psi_n(r) = \left(\frac{\zeta}{1-q}\right)^n \left[\frac{r^{n-1}}{(n-1)!} + \frac{h\zeta}{1-q}\frac{r^n}{n!}\right]e^{-\zeta r}. \tag{15}$$

We anticipate that the LPA does not capture correctly the $r < \Delta$ trend at high densities, while it works well for $r > \Delta$. The reason for this can be traced back to the failure of the LPA to account for the discontinuous slope of the cavity function $y(r)$ at $r=\Delta$. Moreover, the approximate $y(r)$ turns out to be discontinuous rather than continuous at $r=\lambda$, as detailed in Appendix A. These deficiencies can be accounted for step by step at the price of an increase in the complexity of the approximation and are a consequence of the phenomenological nature of the LPA. This will be further discussed in Sec. VII.

As already remarked, the PSW model reduces in the appropriate limit to the penetrable analog of Baxter's sticky hard spheres, denoted as SPS in Ref. 10. This is further elaborated in Appendix B, where it is also discussed the LPA of the SPS model. We explicitly checked this is indeed the limit for PSW in the limit of very narrow and very deep well. On the other hand, we also found (see Appendix B) that this model is also thermodynamically unstable as it violates the stability criterion $\epsilon_r > 2\epsilon_a$, and hence it will not be further discussed in the remaining of this paper.

B. The penetrable-rod limit

Here we show that either in the limit $\epsilon_a \to 0$ (which implies $\gamma \to 0$) or, alternatively, in the limit $\Delta \to 0$, the LPA that we just found for the PSW model reduces to the corresponding one proposed in Ref. 7 for the PS model.

Taking the limit $\gamma \to 0$ in Eq. (7) one finds Eq. (2.53) of Ref. 7. Moreover $q \to 0$ and $h \to (\gamma_r^{-1}-1)e^{\zeta}$ and so Eq. (10) reduces to $\rho = [1+(\gamma_r^{-1}-1)e^{\zeta}]/(1+\zeta^{-1})$, which can be rewritten as $(\xi-\zeta)e^{-\zeta}/(\gamma_r^{-1}-1)=\zeta$ with $\xi=\rho(1+\zeta)$, which coincides with Eq. (4.4) of Ref. 7 where our ζ replaces their ξ'. It is straightforward to check that the same expressions for $\widetilde{\Omega}(s)$ and for ρ in terms of ζ and γ_r are obtained in the alternative limit $\Delta \to 0$. Hence LPA for PS is fully recovered.

C. Comparison with exact low-density expansion

It proves interesting to compare the LPA to order ρ with the exact results derived in Ref. 10 based on a low-density expansion, in order to assess the ability of LPA to reproduce low-density results. The general expansion of $g(r)$ in powers of the density ρ has the following structure:[25]

$$g(r) = g_0(r) + g_1(r)\rho + \cdots. \tag{16}$$

The exact results for $g_0(r)$ and $g_1(r)$ have been derived in Ref. 10:

$$g_0^{\text{exact}}(r) = \begin{cases} 1-\gamma_r, & r < 1, \\ 1+\gamma\gamma_r, & 1 < r < 1+\Delta, \\ 1, & r > 1+\Delta, \end{cases} \tag{17}$$

$$g_1^{\text{exact}}(r) = \gamma_r^2 \begin{cases} (1-\gamma_r)[2(1+\gamma^2\Delta)-r(1+2\gamma+2\gamma^2)], & 0 \le r \le \Delta, \\ (1-\gamma_r)(2-2\gamma\Delta-r), & \Delta \le r < 1, \\ (1+\gamma\gamma_r)(2-2\gamma\Delta-r), & 1 < r < 1+\Delta, \\ 2-2\gamma\Delta-r, & 1+\Delta < r \le 2, \\ \gamma(2+\gamma)(r-2)-2\gamma\Delta, & 2 \le r \le 2+\Delta, \\ (2+2\Delta-r)\gamma^2, & 2+\Delta \le r \le 2+2\Delta, \\ 0, & 2+2\Delta \le r. \end{cases} \tag{18}$$

In order to compare $g_0^{\text{exact}}(r)$ and $g_1^{\text{exact}}(r)$ with LPA results, we expand ζ as derived from Eq. (10) to lowest order in density, $\zeta = \zeta_0\rho + \zeta_1\rho^2 + \mathcal{O}(\rho^3)$, and plug the results into Eqs. (14) and (15). This yields Eq. (16), where the coefficients $g_0(r)$ and $g_1(r)$ are computed within the LPA. Whereas $g_0(r) = g_0^{\text{exact}}(r)$, $g_1(r)$ is found to differ from the exact result $g_1^{\text{exact}}(r)$. Analytical expressions for ζ_0, ζ_1, and $g_1(r)$ can be found in Appendix C.

Having done this, one can estimate the difference in the cavity function between LPA and exact results to order ρ, which reads (see Appendix C)

$$y_1^{\text{exact}}(r) - y_1(r)$$
$$= \begin{cases} C_1 + D_1\Delta + E_1(\Delta-1) + F_1(r-\Delta), & 0 \le r \le \Delta, \\ C_1 + D_1\Delta + E_1(r-1), & \Delta \le r \le 1, \\ C_1 + D_1(1+\Delta-r), & 1 \le r \le 1+\Delta, \end{cases} \tag{19}$$

where

$$C_1 = \gamma\gamma_r^2(1-\gamma_r)\frac{1+\gamma}{1+\gamma\gamma_r}\Delta, \tag{20}$$

$$D_1 = \gamma\gamma_r\frac{(1-\gamma_r)^2}{1+\gamma\gamma_r}, \tag{21}$$

$$E_1 = \gamma_r(1-\gamma_r), \tag{22}$$

$$F_1 = \gamma_r[1-\gamma_r-2\gamma\gamma_r(1+\gamma)]. \tag{23}$$

The right-hand side of Eq. (19) preserves the continuity of $y_1(r)$ at $r = \Delta$ and $r = 1$, but imposes the continuity of $y_1(r)$ at $r = 1+\Delta$ and that of $y_1'(r)$ at $r = 1$ and $r = 1+\Delta$, as well as the discontinuity of the exact $y_1'(r)$ at $r = \Delta$. The latter discontinuity is, according to Eqs. (17) and (18),

$$\lim_{\rho\to 0} \frac{y'(\Delta^+) - y'(\Delta^-)}{\rho y(\Delta)} = 2\gamma\gamma_r^2(1+\gamma). \tag{24}$$

V. THE FISHER–WIDOM LINE

In a remarkable piece of work,[18] Fisher and Widom argued that the asymptotic decay of the correlation functions is determined by the nature of the poles $s_i = s_i(\beta,\rho)$ $(i = 1,2,3,\cdots)$, with largest real part of the Laplace transform $\tilde{G}(s)$ of the RDF. This asymptotic decay can be of two dif-

ferent types: oscillatory at high densities and/or high pressures and monotonic for low densities and/or pressures. The latter regime can exist only in the presence of competing effects in the potential function, so it cannot exist for purely repulsive short-range potentials, such as HS and PS potentials.

In particular, rather general arguments[26] suggest a behavior

$$g(r) - 1 = \sum_i A_i e^{s_i r} \approx A_1 e^{s_1 r}, \tag{25}$$

where we specialized to one-dimensional systems and the sum runs over the discrete sets of poles s_i, A_i being (in general complex) amplitudes. The asymptotic behavior of $g(r)$ is dominated by the pole s_1 having the least negative real part (to ensure stability of the liquid). If s_1 is complex, its conjugate $s_2 = s_1^*$ must also be included in the asymptotic behavior.

Fisher and Widom derived the line—henceforth denoted as Fisher–Widom (FW) line—where this transition takes place, both in the pressure versus temperature and in the density versus temperature diagrams, for the one-dimensional SW potential. On crossing this line, one finds a sharp transition in the character of the RDF $g(r) - 1$: for any fixed temperature in the p-T plane, $g(r)$ has an oscillatory character above the FW line and an exponential decay below it. The transition is a signature of local ordering without any singularities in thermodynamical quantities as there is no phase transition in the one-dimensional SW fluid. In three dimensions, the FW line precedes the coexistence line when lowering the pressure at a fixed temperature. This has been numerically observed for various fluids including SW,[26] Lennard–Jones,[27–29] and other softer potentials.[30]

In view of the possibility for PSW to display fluid-fluid and fluid-solid phase transitions in spite of their one-dimensional character, it is interesting to wonder what happens to the FW line in the transition from SW to PSW. We now analyze this in the framework of the LPA.

The poles of $\tilde{G}(s)$ (different from $s = 0$) can be read off from Eq. (8):

$$\tilde{\Omega}_0(s+\zeta) = \tilde{\Omega}_0(\zeta). \tag{26}$$

As we are here interested in the pole with the negative real part closest to the origin, we set $s = -x \ne 0$ as the real root of Eq. (26),

$$\widetilde{\Omega}_0(\zeta - x) = \widetilde{\Omega}_0(\zeta), \tag{27}$$

and $s = -x' \pm iy$ as the complex root with the least negative real part, i.e.,

$$\mathrm{Re}\,\widetilde{\Omega}_0(\zeta - x' \pm iy) = \widetilde{\Omega}_0(\zeta), \tag{28}$$

$$\mathrm{Im}\,\widetilde{\Omega}_0(\zeta - x' \pm iy) = 0. \tag{29}$$

The pole s_1 determining the asymptotic behavior is either $s_1 = -x$ (monotonic decay) if $x < x'$ or $s_1 = -x' \pm iy$ (oscillatory decay) if $x > x'$. The FW transition takes place when $x = x'$.

Equation (27) yields the condition

$$e^{-s}(1 - qe^{-s\Delta}) = (1 - q)\left(1 + \frac{s}{\zeta}\right), \tag{30}$$

where q is given by Eq. (11). Quite interestingly, as the parameter h is missing, this equation formally coincides with its SW counterpart, originally studied by Fisher and Widom [see Eq. (3.6) in Ref. 18]. We can rewrite Eqs. (27)–(29) as follows:

$$e^{x}(1 - qe^{x\Delta}) = (1 - q)\left(1 - \frac{x}{\zeta}\right), \tag{31}$$

$$e^{x'}(\cos y - qe^{x'\Delta}\cos \lambda y) = (1 - q)\left(1 - \frac{x'}{\zeta}\right), \tag{32}$$

$$e^{x}(\sin y - qe^{x\Delta}\sin \lambda y) = -(1 - q)\frac{y}{\zeta}. \tag{33}$$

At the FW transition $(x = x')$, Eqs. (31)–(33) form a set of three coupled equations whose solution yields x, y, and ζ as functions of q. Use of Eq. (10) then gives the line in the ρ-T plane.

It proves convenient to eliminate ζ from Eqs. (31) and (32) to obtain

$$x = \frac{1}{\Delta}\ln\frac{1 - \cos y}{q(1 - \cos \lambda y)}, \tag{34}$$

so that from Eqs. (31) and (33) we can now get

$$\zeta = x - y\frac{\cos y - \cos \lambda y}{\sin y - \sin \lambda y + \sin y\Delta}. \tag{35}$$

When Eqs. (34) and (35) are inserted into Eq. (31) we get

$$\sin y - \sin \lambda y + \sin y\Delta - \frac{y}{x}(\cos y - \cos \lambda y)$$

$$= -e^{-x}(1 - q)\frac{y}{x}(1 - \cos \lambda y), \tag{36}$$

where $x(q, y)$ is given by Eq. (34) so that this is a transcendental equation in $y(q)$. Once $y(q)$ is known from Eq. (36),

Eqs. (34) and (35) provide $x(q)$ and $\zeta(q)$, respectively. The parameter $\gamma(q)$ is obtained by inverting Eq. (11),

$$\gamma(q) = \frac{q}{e^{-\zeta(q)\Delta} - q}, \tag{37}$$

and the inverse temperature $\beta(q)$ is obtained from

$$\gamma(q) = \frac{e^{\beta(q)\epsilon_a} - 1}{1 - e^{-\beta(q)\epsilon_r}} \tag{38}$$

on using the definitions of γ, γ_r, and γ_a.

Finally, Eqs. (10) and (12) provide $\rho(q)$ and the combination of $\beta(q)$ and $\rho(q)$ yields the FW line in the ρ-T plane. In order to have it in the p-T plane one needs to get before the equation of state and the result will depend on the chosen route (virial, compressibility, or energy). This is discussed in the following section.

VI. EQUATION OF STATE

As PSW is not an exactly solvable model, thermodynamics will in general depend on the followed route, so we are going to check the three standard routes (virial, compressibility, and energy) for the compressibility factor $Z = \beta p / \rho$, as predicted by the LPA. The virial route is defined by

$$Z = 1 - \rho\beta\int_0^\infty dr\,ry(r)e^{-\beta\phi(r)}\phi'(r), \tag{39}$$

which, using standard manipulations,[25] yields

$$Z = 1 + \rho\gamma_r[(1 + \gamma)y(1) - \gamma\lambda y(\lambda)]. \tag{40}$$

As $y(\lambda^-) \neq y(\lambda^+)$ within LPA (see Appendix A), $y(\lambda) = (1/2)[y(\lambda^-) + y(\lambda^+)]$ is assumed. Thus, using Eqs. (A4) and (A8), we get

$$Z = 1 + \frac{\zeta}{1 - q}\left\{1 - \lambda q\left[1 + \gamma_r(1 + \gamma)\frac{1 + \gamma\gamma_r/2}{1 + \gamma\gamma_r}\frac{h\zeta\Delta}{1 - q}\right]\right\}. \tag{41}$$

It is easy to check using Eqs. (10) and (41) that in the case of the SW model $(h = 0)$ one recovers the expected result $Z = \zeta / \rho$.

Next we consider the compressibility route:

$$\chi \equiv \frac{1}{\beta}\left(\frac{\partial\rho}{\partial p}\right)_\beta$$

$$= 1 + 2\rho\int_0^\infty dr[g(r) - 1]$$

$$= 1 + 2\rho\lim_{s\to 0}[\widetilde{G}(s) - s^{-1}]. \tag{42}$$

Using Eqs. (10) and (13) the last term of Eq. (42) can be written as

$$2\rho \lim_{s \to 0}[\tilde{G}(s) - s^{-1}] = \left(\frac{\partial \rho}{\partial \zeta}\right)_\beta - \frac{\tilde{\Omega}'(\zeta)}{\tilde{\Omega}_0'(\zeta)}. \tag{43}$$

Introducing the quantity

$$X(\zeta) \equiv \frac{1}{(\partial \rho/\partial \zeta)_\beta} \frac{\tilde{\Omega}_0'(\zeta) - \tilde{\Omega}'(\zeta)}{\tilde{\Omega}_0'(\zeta)}, \tag{44}$$

Eq. (42) becomes

$$\chi = \left(\frac{\partial \rho}{\partial \zeta}\right)_\beta [1 + X(\zeta)], \tag{45}$$

and using the definition of χ we find

$$\beta\left(\frac{\partial p}{\partial \zeta}\right)_\beta = \frac{1}{1 + X(\zeta)}. \tag{46}$$

Therefore the compressibility route yields

$$\beta p(\zeta) = \int_0^\zeta \frac{d\zeta'}{1 + X(\zeta')}. \tag{47}$$

In the SW limit one clearly has $X(\zeta) = 0$ and $\beta p = \zeta$, as it should.

The energy route is by far the most delicate. We start from the internal energy per particle

$$u = \frac{1}{2\beta} + \rho \int_0^\infty dr \phi(r)g(r)$$
$$= \frac{1}{2\beta} + \epsilon_r \rho \int_0^1 dr g(r) - \epsilon_a \rho \int_1^\lambda dr g(r). \tag{48}$$

Equation (A1) provides the necessary result for $g(r)$ in the interval $0 < r < \lambda$, so that

$$u = \frac{1}{2\beta} + \epsilon_r \frac{h}{1-q}(1 - e^{-\zeta})$$
$$- \epsilon_a\left[\frac{1}{1-q}(1 - e^{-\zeta\Delta})\left(1 + \frac{h}{1-q} + he^{-\zeta}\right)\right.$$
$$\left. - \frac{h}{(1-q)^2}e^{-\zeta\Delta}\zeta\Delta\right]. \tag{49}$$

In order to obtain βp from u we exploit the following thermodynamic relation

$$\rho^2\left(\frac{\partial u}{\partial \rho}\right)_\beta = \left(\frac{\partial \beta p}{\partial \beta}\right)_\rho, \tag{50}$$

and the identity

$$\left(\frac{\partial u}{\partial \rho}\right)_\beta = \left(\frac{\partial u}{\partial \zeta}\right)_\beta\left(\frac{\partial \zeta}{\partial \rho}\right)_\beta, \tag{51}$$

to obtain

$$\left(\frac{\partial \beta p}{\partial \beta}\right)_\rho = \frac{\rho^2}{(\partial \rho/\partial \zeta)_\beta}\left(\frac{\partial u}{\partial \zeta}\right)_\beta. \tag{52}$$

Once again one can check that Eq. (52) is satisfied by the SW result $\beta p = \zeta$.

The right-hand side of Eq. (52) is a function of β and ρ, which we denote as $R(\beta, \rho)$, as ζ is itself a function of the same variables through Eq. (10). Thus, Eq. (52) gives

$$\beta p(\beta, \rho) = \zeta(\rho, \beta_{max}) - \int_\beta^{\beta_{max}} d\beta' R(\beta', \rho), \tag{53}$$

where β_{max} is a conveniently chosen high value.[31]

VII. RELIABILITY OF LPA AND POSSIBLE IMPROVEMENTS

We are now in the position to draw a qualitative phase diagram in the $\rho\sigma - k_B T/\epsilon_a$ plane indicating the boundary where the LPA can be approximately regarded to be reliable. Of course, a definite reliability test is only possible after comparison with computer simulation results but before that we can use the internal consistency among the three thermodynamic routes as a reliability criterion.

In general, it turns out that thermodynamic inconsistency increases as the temperature and the density increase. To characterize this, let us define a density $\rho_{lim}(T)$ such that the largest relative deviation among the three routes is smaller than 5% if $\rho < \rho_{lim}(T)$. Therefore, all the points in the temperature-density plane with $\rho < \rho_{lim}(T)$ represent states where the LPA is only weakly inconsistent. This boundary line is shown in Fig. 2 for three representative cases of the pair (ϵ_r/ϵ_a and Δ). We observe that the region where the LPA is thermodynamically consistent shrinks as ϵ_r/ϵ_a decreases and/or Δ increases. In any case, it is noteworthy that if the density is smaller than a certain value (which of course depends on ϵ_r/ϵ_a and Δ), the LPA remains thermodynamically consistent even for high temperatures.

The above reliability criterion is based on thermodynamics and thus it is a global one. On the other hand, we know that the LPA has some local shortcomings, such as an artificial discontinuity of the cavity function at the point $r = 1 + \Delta$, as shown in Appendix A. Moreover, it does not predict
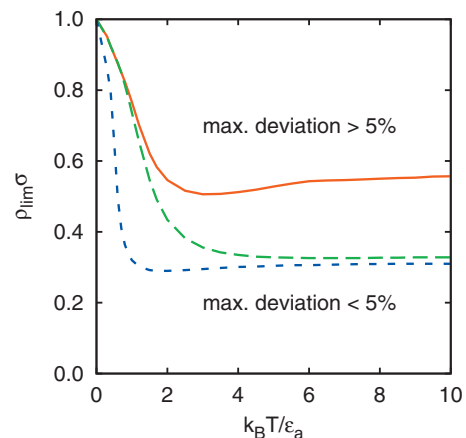

FIG. 2. Phase diagram in the $\rho\sigma - k_B T/\epsilon_a$ space showing the region where LPA can be considered as reliable. The curves correspond, from top to bottom, to the cases $(\epsilon_r/\epsilon_a, \Delta) = (5, 0.5)$, $(5, 1)$, and $(2, 0.5)$. The points below each curve represent states where the relative deviation between the three routes to the pressure is smaller than 5%.

the discontinuity of the slope of the RDF at $r = \Delta$, already present by the exact result to first order in density, as indicated by Eq. (24).

As anticipated in Sec. IV, we can extend the validity of the LPA by a suitable modification of the cavity function $y(r)$ in order to ensure a correct behavior both within the core

region and at the well-edge discontinuity. We outline a possible approach to this issue in the remainder of this section.

Inspired by the comparison with exact low-density results as given in Sec. IV C, we modify the LPA (mLPA) by adding linear terms in the region $0 \leq r \leq 1 + \Delta$, following a form based on that of Eq. (19), namely,

$$g^{\text{mLPA}}(r) = g(r) + \frac{1}{\rho} \begin{cases} (1 - \gamma_r)[C + D\Delta + E(\Delta - 1) + F(r - \Delta)], & 0 \leq r \leq \Delta, \\ (1 - \gamma_r)[C + D\Delta + E(r - 1)], & \Delta \leq r < 1, \\ (1 + \gamma\gamma_r)[C + D(1 + \Delta - r)], & 1 < r < 1 + \Delta, \end{cases} \tag{54}$$

where $g(r)$ is the LPA RDF as given Eq. (14). The parameters C, D, and E can be determined by imposing the continuity of $y(r)$ at $r = 1 + \Delta$ and of $y'(r)$ at $r = 1 + \Delta$ and $r = 1$, respectively. They are given by

$$C = \frac{\gamma_r(1 + \gamma)}{1 + \gamma\gamma_r} \frac{hq\zeta^2}{(1 - q)^2} \Delta, \tag{55}$$

$$D = \frac{1 - \gamma_r}{1 + \gamma\gamma_r} \frac{hq\zeta^2}{(1 - q)^2} + C\zeta, \tag{56}$$

$$E = \frac{1}{1 + \gamma\gamma_r} \frac{h\zeta^2}{(1 - q)^2} - D. \tag{57}$$

The addition of the coefficient F is motivated by the exact results to first order in density, Eq. (18), showing that, as recalled above, $g(r)$ exhibits a change of slope at $r = \Delta$, a feature not accounted for by the LPA. In order to determine the coefficient F we extend the exact low-density condition (24) to finite density. This implies

$$F = E - 2\rho\gamma\gamma_r^2(1 + \gamma)\left[\frac{1 + \gamma}{\gamma(1 - \gamma_r)} \frac{hq\zeta}{1 - q} + C + D\Delta \right.$$
$$\left. + E(\Delta - 1) \right]. \tag{58}$$

It is straightforward to check that $C = C_1\rho^2 + \mathcal{O}(\rho^3)$, $D = D_1\rho^2 + \mathcal{O}(\rho^3)$, $E = E_1\rho^2 + \mathcal{O}(\rho^3)$, $F = F_1\rho^2 + \mathcal{O}(\rho^3)$, where C_1, D_1, E_1, and F_1 are given by Eqs. (20)–(23). Therefore, the mLPA is exact to first order in density.

The discussed modification of LPA then takes care of the continuity of the cavity function $y(r)$ at both interaction discontinuities $r = 1$ (already accounted for within LPA) and $r = \lambda$ (where the original LPA fails to provide continuity), and it correctly matches the exact results for $g(r)$ up to first order in density. A similar modification of the SPS model, discussed in Appendix A, would heal the discontinuity appearing in the corresponding LPA values $y^{\text{SPS}}(1^+) \neq y^{\text{SPS}}(1^-)$, which is a consequence of the combined effects of the LPA discontinuity $y(\lambda^+) \neq y(\lambda^-)$ and the sticky limit. This would provide an expression (not reported here) which is this sticky limit of Eq. (54).

VIII. MONTE CARLO SIMULATIONS AND INTEGRAL EQUATION THEORY

In order to assess the reliability of the LPA, we will compare in Sec. IX with specialized MC simulations. In addition, prompted by the results of Ref. 10, we will also compare LPA with standard integral equation theories, such as PY and HNC.[25]

A. Monte Carlo simulations

We employed the conventional MC simulation on an *NVT* ensemble with periodic boundary conditions which in one dimension means that the system is treated as a ring. $N = 5 \times 10^4$ penetrable-rod particles were displaced according to the Metropolis algorithm to create an initial sample of configurations. Following the equilibration stage, each run is divided into 20 basic simulation blocks, in which 10^5 measurements are performed to collect correlation functions data. One hundred trial moves per particle are implemented between each measurement, so that 10^{13} equilibrium configurations are generated in each run.

In order to speed up the simulation process the particles are labeled such that they create a consecutive sequence in clockwise order. Calculation of a potential of a particle i in a given configuration then reduces to a searching for the highest label $j > i$ and the lowest label $k < i$ associated with the particles still interacting with the particle i. In contrast with the case of impenetrable spheres in one dimension, the order of particles changes so that a relabeling must be undertaken after each shift of a particle. Obviously, at higher temperatures the number of penetration can be high, which makes the calculations more demanding compared to hard body systems.

There are in general two routes for the evaluation of the pressure. Determination of the pressure using a mechanical (virial) route relies on an ensemble average of a virial, i.e., a quantity involving the forces acting on all the particles. Alternatively, a thermodynamic expression relates pressure to the volume derivative of the free energy and is implemented by calculating the free energy change associated with small virtual change of volume. However, for systems with discontinuous interaction. both mechanical and thermodynamic ap-
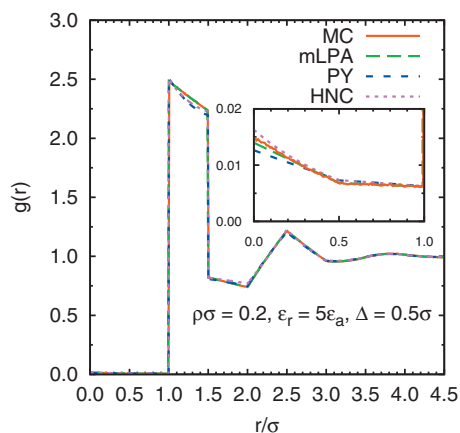
FIG. 3. Results for the RDF $g(r)$ vs r/σ with $\Delta/\sigma=0.5$, $k_BT/\epsilon_a=1$, $\epsilon_r/\epsilon_a=5$, and $\rho\sigma=0.2$. Predictions from the mLPA given by Eq. (54) (long dashed line) are compared with both MC results (solid line) and PY and HNC integral equations (short dashed and dotted lines, respectively). In the inset a magnification of the $r<\sigma$ region is shown.

proaches become identical. Specifically, for the PSW fluid model both approaches reduce on a calculation of distribution function at $r=1$ and $r=\lambda$ [see Eq. (40)].

B. Integral equations

The presence of penetrability does not pose any particular difficulties to standard integral equation theories. As a matter of fact these have been already employed in the PS case[7] and in the PSW case[10] within standard approximations where the one-dimensional Ornstein–Zernike equation,

$$h(r) = c(r) + \rho \int_{-\infty}^{\infty} dr' c(|r-r'|)h(r'), \tag{59}$$

is associated with a PY closure,

$$c(r) = f(r)y(r), \tag{60}$$

or with an HNC closure

$$c(r) = f(r)y(r) + y(r) - 1 - \ln y(r). \tag{61}$$

We solved the PY and HNC integral equations using a Zerah's algorithm[32] with up to 2^{12} grid points depending on the considered state point.

IX. RESULTS WITHIN THE LPA

In this section we compare numerical results stemming from the LPA with MC simulations and integral equation theories (PY and HNC) for both RDF (where we will consider the improved mLPA) and equation of state (at the level of the simple LPA).

A. Results for $g(r)$

As a first approach to assess the performance of the LPA, we consider the RDF $g(r)$ for two representative state points. The well is kept fixed at $\Delta/\sigma=0.5$ and temperature is also fixed by the attractive energy scale so that $k_BT/\epsilon_a=1$. Figure 3 depicts the behavior of $g(r)$ for a density $\rho\sigma=0.2$ and an
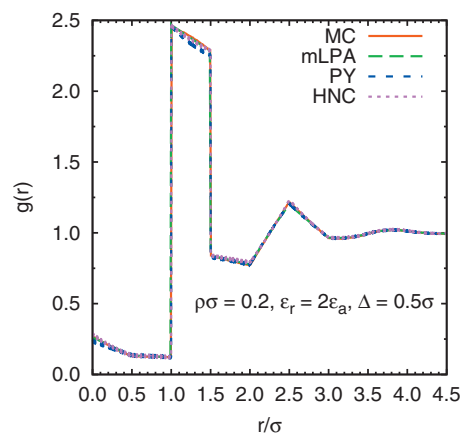
energy ratio $\epsilon_r/\epsilon_a=5$, which is well above the stability threshold value $\epsilon_r/\epsilon_a=2$.[10] The stability threshold is then probed in Fig. 4, whereas a higher density $\rho\sigma=0.8$ is tested in Fig. 5 with all other parameters identical to those of Fig. 3.

In all cases, mLPA results (that only differ from the LPA ones within the interaction range, $0<r<\lambda$) are compared with MC simulations and integral equations and follow the expected trend. For low densities ($\rho\sigma=0.2$) and low penetrability ($\epsilon_r/\epsilon_a=5$) mLPA, PY, and HNC all provide very accurate descriptions of MC data with a very tiny difference in the well region $1\leq r/\sigma\leq 1.5$, where the integral equations predict a slight curvature of $g(r)$, while the mLPA confirms the practically linear shape of the simulation data. Moreover, a blow up of $g(r)$ in the deep core region ($0\leq r\leq\Delta$) shows that the mLPA is very accurate, while the PY and HNC theories underestimate and overestimate, respectively, the MC data. The same good performance of the mLPA is also observed for a much larger penetrability ($\epsilon_r/\epsilon_a=2$), provided the density is relatively low ($\rho\sigma=0.2$), as shown in Fig. 4. This is consistent with Fig. 2, according to which the density $\rho\sigma=0.2$ lies in the region where the LPA is expected to be accurate for any temperature when $\epsilon_r/\epsilon_a=2$ and $\Delta/\sigma=0.5$. As for the integral equations, they are also rather accurate for the case considered in Fig. 3, although they still show a slight curvature inside the well and slightly deviate from the

FIG. 4. Same as in Fig. 3 at the instability threshold $\epsilon_r/\epsilon_a=2$. All other parameters are as in Fig. 3.
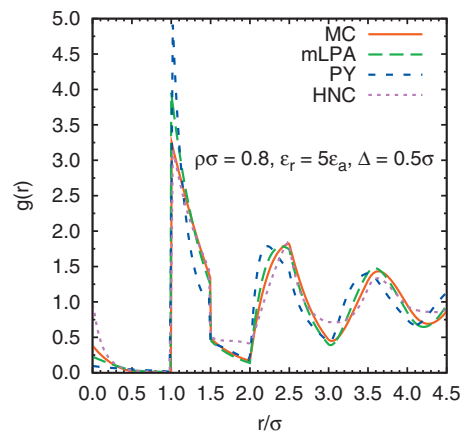

FIG. 5. Same as in Fig. 3 at a higher density $\rho\sigma=0.8$. All other parameters are as in Fig. 3.
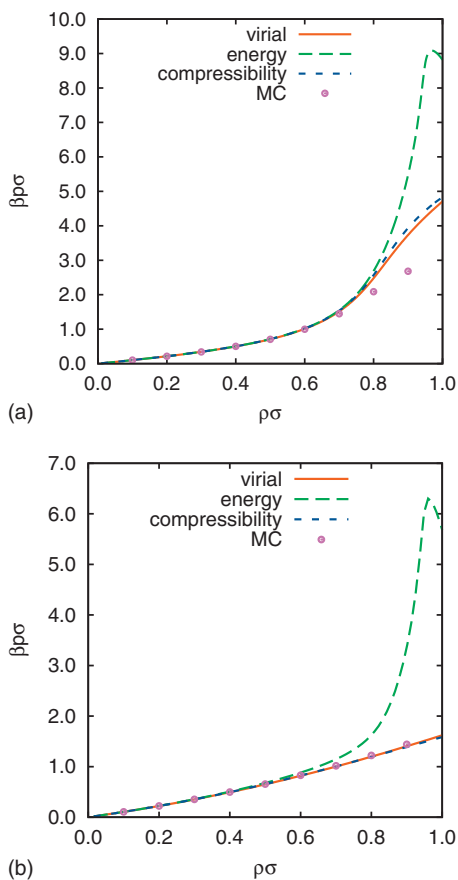
FIG. 6. Plot of $\beta p \sigma$ vs $\rho \sigma$ for $\Delta / \sigma = 0.5$, $\epsilon_r / \epsilon_a = 5$, and $k_B T / \epsilon_a = 1$ (top panel) and $k_B T / \epsilon_a = 5$ (bottom panel). Different curves refer to different routes. The symbols denote MC simulation results.

FIG. 7. Same as in Fig. 6, except that $\epsilon_r / \epsilon_a = 2$.

MC results for $r < \Delta$. Differences begin to be relevant at high-density ($\rho \sigma = 0.8$), mostly inside the core $0 < r / \sigma < 1$ and in the contact values $r = \sigma^+$. Again, this agrees with Fig. 2, which shows that the state $(\rho \sigma, k_B T / \epsilon_a) = (0.8, 1)$ is practically on the boundary line corresponding to $\epsilon_r / \epsilon_a = 5$ and $\Delta / \sigma = 0.5$. In any case, Fig. 5 shows that the best general agreement with the MC results is presented by the mLPA, followed by the HNC theory, which, however, predicts reasonably well the peaks of $g(r)$, but not the minima. We explicitly checked (not shown) that for smaller values of the well width Δ, PSW results increasingly tend to the SPS counterpart, as anticipated.

B. Results for equation of state

Next we turn to the analysis of thermodynamics within LPA. As anticipated (see Sec. VI), the lack of an exact solution gives rise to thermodynamical inconsistencies where compressibility, virial, and energy routes all give rise to different results. The consistency degree among different routes is a (partial) signature of the LPA performance, as discussed in Sec. VII. In Fig. 6 we report the behavior of βp as a function of the reduced density $\rho \sigma$. Once again, we fix the width of the well $\Delta = 0.5 \sigma$ and the energy ratio $\epsilon_r / \epsilon_a = 5$ and consider two different temperatures $k_B T / \epsilon_a = 1$ (top panel) and $k_B T / \epsilon_a = 5$ (bottom panel). In the former case different
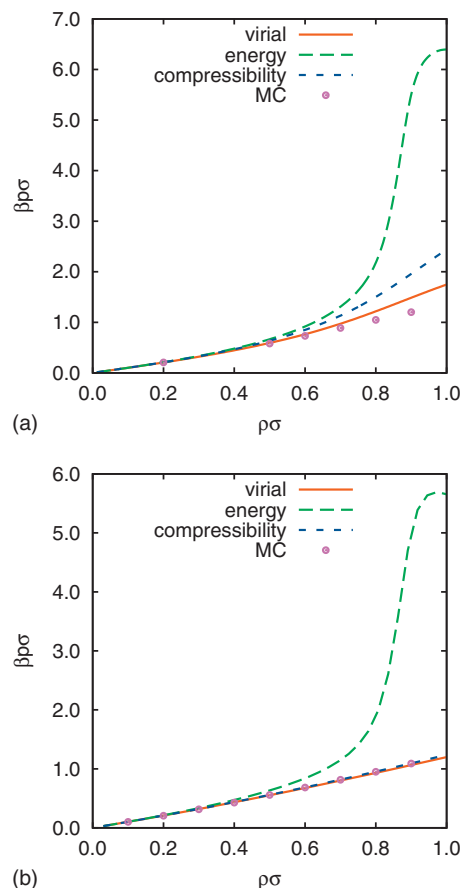
routes give practically indistinguishable results up to $\rho \sigma \approx 0.8$, whereas in the latter a difference is clearly visible at densities higher than $\rho \sigma \approx 0.6$ with energy, virial, and compressibility routes having decreasing βp for identical values of $\rho \sigma$. Similar results are observed at the stability edge $\epsilon_r / \epsilon_a = 2$, as shown in Fig. 7. We remark that higher temperatures effectively correspond to higher penetrability, as particles have relatively more attractive energies, as compared to the positive repulsive barrier, and hence they can compenetrate more. Therefore pressure differences among different thermodynamical routes can be reckoned as a rough measure of the breakdown of LPA. On the other hand, consistency among different routes does not necessarily means "exact" results, as they can all converge to the incorrect value.

A comparison with MC numerical simulations is therefore also included in Figs. 6 and 7. Somewhat surprisingly, this suggests that the virial route is the closest to the true value for the pressure, with both compressibility and energy routes always lying on the opposite side with the latter being the farthest from the MC results.

In order to compare with LPA, we carefully scanned a wide range of temperatures and densities within the region $0 \le \rho \sigma \le 1$ where LPA provides consistent thermodynamics as remarked. Within this region we found no signature of fluid-fluid transition line as expected. Our preliminary numerical results for higher densities, where strong overlapping among different particles is enforced, provide a clear evi-
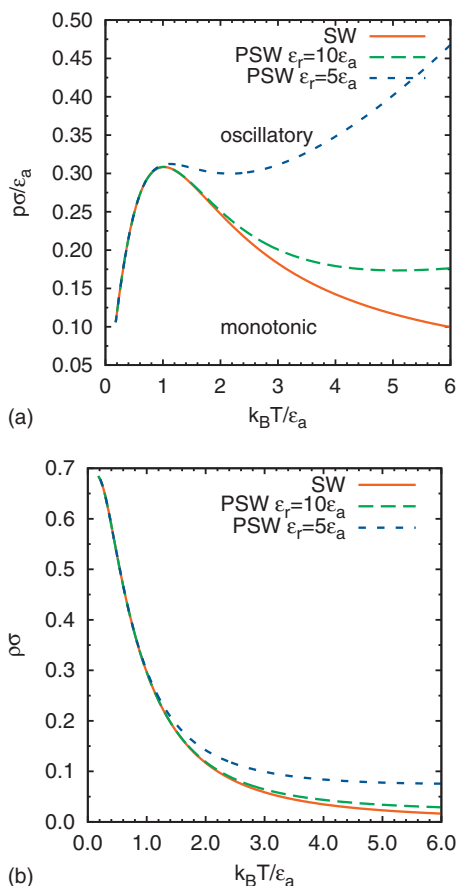
FIG. 8. Plot of the FW transition line in the $p\sigma/\epsilon_a$ vs k_BT/ϵ_a plane (top panel) and in the $\rho\sigma$ vs k_BT/ϵ_a plane (bottom panel). Here $\Delta/\sigma=1$ and $\epsilon_r/\epsilon_a=(\infty,10,5)$. Note that, except in the SW case ($\epsilon_r/\epsilon_a=\infty$), $\zeta/\sigma \neq \beta p$. Note also that in these cases the three routes to the pressure are not distinguishable one from the other on the graph scale.

FIG. 9. Same as in Fig. 8, except that $\Delta/\sigma=0.5$.

dence of phase separation. As the main emphasis of the present paper is on analytical approximations, this point will be discussed in some detail elsewhere.

C. Results for Fisher–Widom line

Let us follow the recipe given in Sec. V to locate the FW line. In Fig. 8 we report the quantities $p\sigma/\epsilon_a$ and $\rho\sigma$ as a function of k_BT/ϵ_a for $\Delta=\sigma$ and decreasing values of the ratio ϵ_r/ϵ_a. The case $\epsilon_r/\epsilon_a \to \infty$ is the one addressed in the original FW work on the one-dimensional SW fluid.[18] We remind that above the FW line, $g(r)-1$ has oscillatory behavior, whereas it is exponentially decaying below it, and it is located in the homogeneous fluid region of the phase diagram, above the critical temperature if phase separation is present.

As the repulsive barrier becomes finite, the region of monotonic behavior increases for large k_BT/ϵ_a whereas it remains essentially unchanged for lower temperatures. This is not surprising as penetrability (i.e., finite repulsive barrier) favors the onset of a critical region. Somewhat more surprising is the fact that this happens in the high- rather than in the low-temperature region. A similar feature is also appearing in the ρ-T plane (see bottom panel). In order to test the effect of different width values, we repeated the same calculation for $\Delta=0.5\sigma$. Results are presented in Fig. 9 and are in agreement
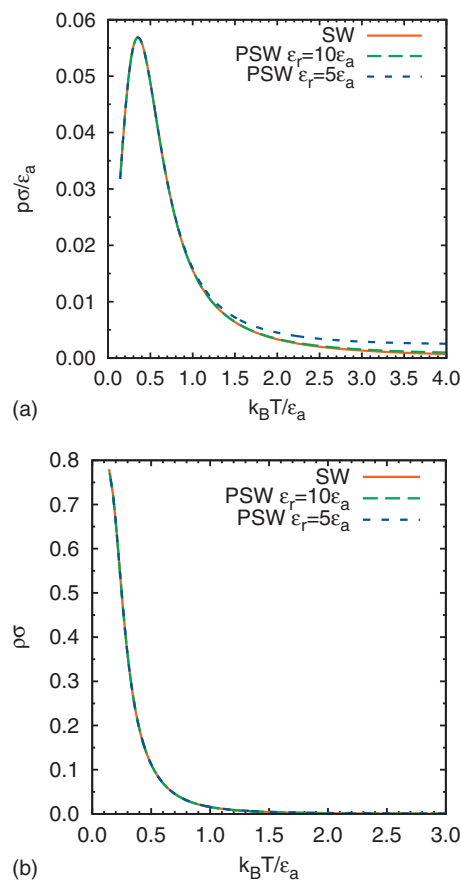
(in the limit $\epsilon_r/\epsilon_a \to \infty$) with results for the one-dimensional SW fluid presented in Ref. 33 for a hard-core to well-width ratio equal to 2 (see Fig. 1 in Ref. 33). For this well width the influence of the ratio ϵ_r/ϵ_a on the FW line is much less important.

Although we have been unable to find a simple physical explanation for this behavior, we remark that the sensitivity of the FW line to the barrier height occurs as the density decreases. Consider for instance the density $\rho\sigma=0.1$ for models with $\Delta=\sigma$. In the SW case ($\epsilon_r/\epsilon_a \to \infty$) the decay of the RDF changes from monotonic to oscillatory as one increases the temperature and crosses the value $k_BT/\epsilon_a \simeq 2.2$. In the case of the PSW model with $\epsilon_r/\epsilon_a=5$, according to the LPA, the transition takes place at $k_BT/\epsilon_a \simeq 2.8$. If the density is sufficiently low ($\rho\sigma \lesssim 0.076$ for $\epsilon_r/\epsilon_a=5$), the asymptotic decay of $g(r)-1$ is monotonic for any temperature, while this effect is absent in the impenetrable SW limit. One might argue that this influence of the energy ratio ϵ_r/ϵ_a on the high-temperature branch of the FW line is an artifact of the LPA since the latter approximation is *a priori* restricted to low temperatures. On the other hand, this high-temperature branch also corresponds to low densities, counterbalancing the penetrability effect and making the LPA presumably accurate. As a matter of fact, the FW lines plotted in the top panels of Figs. 8 and 9 are obtained from the three thermodynamic routes but the three curves are, in each case, indistinguishable from each other. In other words, the FW lines are well inside the regions in Fig. 2 where the LPA is thermodynamically consistent from a practical point of view.

X. CONCLUSIONS AND OUTLOOK

One-dimensional fluids with nearest-neighbor interactions admit an exact analytical solution for both structural and thermophysical properties with a well defined protocol.[5,20] Nearest-neighbor interactions, in turn, require a well defined hard-core term in the pairwise potential preventing superpositions and particle exchanges which is the crucial ingredient necessary for the exact solution. The absence of the above constraint, on the other hand, allows the presence of critical phase transitions, in spite of the one-dimensional character of the system, which are fully absent in the hard-core counterparts.

Effective pair interactions with a soft-repulsive component are well-known features of polymer solutions and colloidal suspensions.[1,2] Among many different model potentials,[2] with various degrees of core softness, PSs stands out for its simplicity.[7] In this model, the infinite repulsive energy is reduced to a finite one, thus introducing an effective "temperature" into an otherwise athermal hard-sphere system. This potential model lacks attractive interactions but these can be accounted for in the PSW companion model where an attractive short-range SW is added to the PS model.[10]

At sufficiently low temperatures, thermal energy cannot overcome the repulsive barrier and penetrability is low, whereas at high temperatures different particles can interpenetrate to a significant extent. Hence, within this framework, low- and high-temperature and low- and high-penetrability terminology can be used synonymously.

In this work we studied structural and thermodynamic properties of the PSW model. Using a LPA akin to that discussed for PS,[7] we considered rather interesting issues specific of the presence of attractive interactions (and thus absent in the PS model) such as fluid-fluid phase separation or the existence of a FW line.[18] This is a pseudotransition associated with a clear-cut change, from oscillatory to monotonic, in the asymptotic decay properties of the RDF, as transition line is approached, even in those cases where the existence of a critical region is prevented by rigorous theorems (e.g., the SW one-dimensional fluid). It requires the simultaneous presence of attractive and repulsive energies and hence it cannot exist for the simpler PS model

Our LPA has been devised to reduce to that of PS in the limit of no well. We assessed its performance by comparing it with exact results[10] in the low-density limit and by comparing with MC simulations and PY and HNC integral equation theories for larger densities where exact analytical results do not exist. We found that it reproduces a significant portion of the T-p parameter space at the level of pair correlation function, the main difference being in the penetrability region $0 < r < \sigma$. At odds with its SW counterpart, PSW thermodynamics depends on the chosen route in view of the inconsistencies introduced by the LPA. We quantified the inconsistencies among virial, compressibility, and energy routes and discussed how they reflect into the computation of the FW line. In all considered cases, we found a magnification at large temperatures of the monotonic regime region as penetrability increases and a much smaller, if any, modifica-

tion, at lower temperatures. In all cases the FW line is found within the region where LPA is expected to be accurate as thermodynamic inconsistencies are small. Within the density region $0 \leq \rho\sigma \leq 1$, we found no sign of a fluid-fluid phase separation, although both fluid-fluid and fluid-solid transitions are expected at higher densities.

In the limit of infinitely narrow and deep well, PSW has been shown to reduce to a penetrable version of Baxter adhesive model,[34] which violates the stability condition set for a well defined thermodynamic limit.[10] As the main weaknesses of LPA for the PSW stems mainly from a nonadequate representation of the penetrable region $0 < r/\sigma < 1$, we then discussed how a simple modification of the RDF in this region gives a significant improvement when tested against MC results under rather demanding conditions.

This paper is part of an ongoing effort on PSW outlined in our previous work.[10] Future work will address a complementary approximation (the high-penetrability limit) and its matching with the LPA discussed in the present paper, so that the entire parameter T-p-ρ space can be discussed with some comfortable degree of confidence. This will resolve some of the subtle points with no conclusive answer left by the present paper. In addition, a detailed investigation of the high density region $\rho\sigma > 1$ is underway and will be reported elsewhere.

APPENDIX A: ANALYSIS OF THE CONTINUITY OF $y(r)$ WITHIN LPA

From Eq. (14) we have that if $r < 2$,

$$\rho g(r) = \frac{h\zeta}{1-q} e^{-\zeta r}$$
$$+ \begin{cases} 0, & 0 \leq r < 1, \\ \psi_1(r-1), & 1 < r < 1+\Delta, \\ \psi_1(r-1)q - \psi_1(r-1-\Delta), & 1+\Delta < r < 2. \end{cases}$$

(A1)

The explicit expressions of $\psi_1(r)$ is, from Eq. (15),

$$\psi_1(r) = \frac{\zeta}{1-q} e^{-\zeta r} \left(1 + \frac{h\zeta}{1-q} r \right).$$

(A2)

The continuity condition of $y(r)$ at $r=1$ is then given by condition

$$\frac{1}{1-\gamma_r}\frac{h\zeta}{1-q}e^{-\zeta} = \frac{1}{1+\gamma\gamma_r}\left[\frac{h\zeta}{1-q}e^{-\zeta} + \psi_1(0)\right], \quad (A3)$$

which is identically satisfied, so that

$$\rho y(1) = \frac{\zeta}{(1-q)\gamma_r(1+\gamma)}. \quad (A4)$$

However, $y(r)$ is discontinuous at $r=\lambda=1+\Delta$:

$$\rho y(\lambda^-) = \frac{1}{1+\gamma\gamma_r}\left[\frac{h\zeta}{1-q}e^{-\zeta\lambda} + \psi_1(\Delta)\right]$$

$$= \frac{\zeta q}{\gamma_r\gamma(1-q)}\left[1 + \frac{\gamma_r(1+\gamma)}{1+\gamma\gamma_r}\frac{h\zeta\Delta}{1-q}\right], \quad (A5)$$

$$\rho y(\lambda^+) = \frac{h\zeta}{1-q}e^{-\zeta\lambda} + \psi_1(\Delta) - q\psi_1(0)$$

$$= \frac{\zeta q}{\gamma_r\gamma(1-q)}\left[1 + \gamma_r(1+\gamma)\frac{h\zeta\Delta}{1-q}\right]. \quad (A6)$$

The jump is then given by

$$\rho[y(\lambda^+) - y(\lambda^-)] = \frac{\gamma_r(1+\gamma)}{1+\gamma\gamma_r}\frac{hq\zeta^2\Delta}{(1-q)^2}, \quad (A7)$$

and the value used as an estimate of the point is then given by the average of the left and right limits,

$$\rho\frac{y(\lambda^+) + y(\lambda^-)}{2}$$

$$= \frac{\zeta q}{\gamma_r\gamma(1-q)}\left[1 + \gamma_r(1+\gamma)\frac{1+\gamma\gamma_r/2}{1+\gamma\gamma_r}\frac{h\zeta\Delta}{1-q}\right]. \quad (A8)$$

APPENDIX B: THE STICKY-PENETRABLE-SPHERE MODEL

In this appendix, we provide a connection with the SPS introduced in Ref. 10. This is the penetrable analog of Baxter's sticky-hard-sphere well-known model.[34] The SPS limit can be obtained by considering the limit $\Delta \to 0$ and $\epsilon_a \to \infty$ so that $\alpha = \gamma\Delta$ remains finite, hence playing the role of an adhesivity parameter. We then define SPS by the Mayer function[10]

$$f_{\mathrm{SPS}}(r) = \gamma_r f_{\mathrm{SHS}}(r), \quad (B1)$$

where

$$f_{\mathrm{SHS}}(r) = f_{\mathrm{HS}}(r) + \alpha\delta_+(r-\sigma) \quad (B2)$$

is the Mayer functions of the SHS potential and

$$\delta_+(r) \equiv \lim_{a\to 0^+}\frac{\Theta(r) - \Theta(r-a)}{a}. \quad (B3)$$

The fluid parameters are then the adhesivity coefficient $\alpha > 0$, the penetrability coefficient γ_r, and the density ρ.

As anticipated, the SPS fluid is thermodynamically unstable in the sense discussed in Sec. II. This can be seen both because the required limit does not satisfy the sufficient condition for stability $\epsilon_r > 2\epsilon_a$,[10] and directly using arguments akin to those used by Stell[35] to prove the instability of the

original Baxter's model[34] in dimensions greater than one. Nonetheless it provides an overall consistency testbench to the performance of LPA within the well established framework of SHS.

In the combined limit $\gamma \to \infty$ and $\Delta \to 0$ with $\alpha = \gamma\Delta$, Eqs. (7) and (9) become

$$\widetilde{\Omega}^{\mathrm{SPS}}(s) = \frac{1-\gamma_r}{s} + \gamma_r\left(\alpha + \frac{1}{s}\right)e^{-s}, \quad (B4)$$

$$\widetilde{\Omega}_0^{\mathrm{SPS}}(s) = \gamma_r\left(\alpha + \frac{1}{s}\right)e^{-s}. \quad (B5)$$

Using the first equality in Eq. (10) it follows that

$$\rho = \frac{f/\zeta + 1/\zeta + \alpha}{\alpha + 1/\zeta + 1/\zeta^2}, \quad (B6)$$

where

$$f = \frac{1-\gamma_r}{\gamma_r}e^{\zeta}. \quad (B7)$$

We then use the LPA as given in Eq. (8) to find

$$\rho\widetilde{G}^{\mathrm{SPS}}(s) = \frac{f/(s+\zeta) + [\alpha + 1/(s+\zeta)]e^{-s}}{(\alpha + 1/\zeta) - [\alpha + 1/(s+\zeta)]e^{-s}}, \quad (B8)$$

whose inverse Laplace transform yields the RDF,

$$\rho g^{\mathrm{SPS}}(r) = \sum_{n=0}^{\infty}\psi_n^{\mathrm{SPS}}(r-n)\Theta(r-n), \quad (B9)$$

where

$$\psi_0^{\mathrm{SPS}}(r) = \frac{f}{\alpha + 1/\zeta}e^{-\zeta r}, \quad (B10)$$

$$\psi_n^{\mathrm{SPS}}(r) = \left(\frac{\alpha}{\alpha + 1/\zeta}\right)^n\left[\frac{f}{\alpha + 1/\zeta} + \sum_{k=1}^{n}\binom{n}{k}\frac{1}{\alpha^k k!}\right.$$

$$\left.\times\left(kr^{k-1} + \frac{f}{\alpha + 1/\zeta}r^k\right) + \delta(r)\right]e^{-\zeta r}. \quad (B11)$$

In the impenetrable limit $\gamma_r \to 1$ and $f \to 0$, Eqs. (B6)–(B11) reduce to the exact one-dimensional SHS counterparts,[22,36,37] as they should.

A word of caution is in order here. Using Eqs. (B9)–(B11), the cavity function $y(r) = g(r)e^{\beta\phi(r)}$ at contact $r=1$ is found to be discontinuous as

$$\rho y^{\mathrm{SPS}}(1^-) = \frac{1}{\gamma_r}\frac{1}{\alpha + 1/\zeta}, \quad (B12)$$

$$\rho y^{\mathrm{SPS}}(1^+) = \rho y^{\mathrm{SPS}}(1^-) + \frac{\alpha f}{(\alpha + 1/\zeta)^2}. \quad (B13)$$

Note that Eq. (B12) is the sticky limit of the PSW value $\rho y(1)$, Eq. (A4), [recall that $y(r)$ is continuous at $r=1$ within the PSW] and is also the sticky limit of the PSW value $\rho y(\lambda^-)$, Eq. (A5). On the other hand, Eq. (B13) is the sticky limit of the PSW value $y(\lambda^+)$, Eq. (A5). Therefore, the discontinuity of $y^{\mathrm{SPS}}(r)$ at $r=1$ is a direct consequence of the

discontinuity of the PSW cavity function at $r = \lambda$. Both discontinuities are artifacts of the LPA. Again, this can be amended by an improved mLPA approach which is discussed in Sec. VII.

APPENDIX C: LOW-DENSITY EXPANSION OF THE LPA

Let us compare the LPA to order ρ with the exact results. From Eqs. (10)–(12) we easily get

$$\zeta = \zeta_0 \rho + \zeta_1 \rho^2 + \mathcal{O}(\rho^3), \qquad (C1)$$

with

$$\zeta_0 = \gamma_r, \quad \zeta_1 = \gamma_r^3(1 - \gamma\Delta). \qquad (C2)$$

Upon inserting the result into Eqs. (14) and (15), and after some algebra, we find the correct zeroth order term $g_0(r) = g_0^{\text{exact}}(r)$ as given in Eq. (17), and

$$g_1(r) = \gamma_r^2 \begin{cases} (1 - \gamma_r)\left[1 - \gamma\dfrac{1 + \gamma_r}{\gamma_r}\Delta - (r-1)\dfrac{1}{\gamma_r}\right], & 0 \le r < 1, \\[2mm] (1 + \gamma\gamma_r)\left[1 - \gamma\dfrac{1 + \gamma_r}{\gamma_r}\Delta + (r-1)\dfrac{\gamma - \gamma_r - 2\gamma\gamma_r}{\gamma_r(1 + \gamma\gamma_r)}\right], & 1 < r < 1 + \Delta, \\[2mm] 2 - 2\gamma\Delta - r, & 1 + \Delta < r \le 2, \\[2mm] \gamma(2 + \gamma)(r - 2) - 2\gamma\Delta, & 2 \le r \le 2 + \Delta, \\[2mm] (2 + 2\Delta - r)\gamma^2, & 2 + \Delta \le r \le 2 + 2\Delta, \\[2mm] 0, & 2 + 2\Delta \le r. \end{cases} \qquad (C3)$$

Comparison between Eqs. (C3) and (18) shows that the LPA reproduces the exact result for $r \ge 1 + \Delta$. On the other hand, it fails to do so within the potential range. The differences between the first-order exact and LPA cavity functions are given by Eq. (19).

[1] J.-L. Barrat and J.-P. Hansen, *Basic Concepts for Simple and Complex Liquids* (Cambridge University Press, Cambridge, 2003).

[2] C. N. Likos, Phys. Rep. **348**, 267 (2001).

[3] M. Watzlawek, C. N. Likos, and H. Löwen, Phys. Rev. Lett. **82**, 5289 (1999).

[4] M. Ballauff and C. N. Likos, Angew. Chem., Int. Ed. **43**, 2998 (2004).

[5] Z. W. Salsburg, R. W. Zwanzig, and J. G. Kirkwood, J. Chem. Phys. **21**, 1098 (1953).

[6] See, e.g., R. Fantoni, Ph.D. thesis, University of Trieste, 2003, and references therein.

[7] Al. Malijevský and A. Santos, J. Chem. Phys. **124**, 074508 (2006).

[8] C. N. Likos, M. Watzlawek, and H. Löwen, Phys. Rev. E **58**, 3135 (1998).

[9] A. Lang, C. N. Likos, M. Watzlawek, and H. Löwen, J. Phys: Condens. Matter **12**, 5087 (2000).

[10] A. Santos, R. Fantoni, and A. Giacometti, Phys. Rev. E **77**, 051206 (2008).

[11] D. Ruelle, *Statistical Mechanics: Rigorous Results* (Benjamin, London, 1969).

[12] M. E. Fisher and D. Ruelle, J. Math. Phys. **7**, 260 (1966).

[13] B. Widom and J. S. Rowlinson, J. Chem. Phys. **52**, 1670 (1970).

[14] S. Torquato, J. Chem. Phys. **81**, 5079 (1984).

[15] P. A. Rikvold and G. Stell, J. Chem. Phys. **82**, 1014 (1985).

[16] F. H. Stillinger, J. Chem. Phys. **65**, 3968 (1976).

[17] A. A. Louis, P. G. Bolhuis, and J.-P. Hansen, Phys. Rev. E **62**, 7961 (2000).

[18] M. E. Fisher and B. Widom, J. Chem. Phys. **50**, 3756 (1969).

[19] D. S. Corti and P. G. Debenedetti, Phys. Rev. E **57**, 4211 (1998).

[20] M. Heying and D. S. Corti, Fluid Phase Equilib. **220**, 85 (2004).

[21] It may be noted that the LPA presented here is identical to the low-temperature approximation introduced in Ref. 7.

[22] S. B. Yuste and A. Santos, J. Stat. Phys. **72**, 703 (1993).

[23] A. Santos, Mol. Phys. **104**, 3411 (2006).

[24] See, e.g., A. Giacometti, G. Pastore, and F. Lado, Mol. Phys. **107**, 555 (2009).

[25] J.-P. Hansen and I. R. McDonald, *Theory of Simple Liquids* (Academic, Amsterdam, 2006).

[26] R. Evans, J. R. Henderson, D. C. Hoye, A. O. Parry, and Z. A. Suber, Mol. Phys. **80**, 755 (1993).

[27] R. J. F. Leote de Carvalho, R. Evans, D. C. Hoyle, and J. R. Henderson, J. Phys.: Condens. Matter **6**, 9275 (1994).

[28] C. Vega, L. F. Rull, and S. Lago, Phys. Rev. E **51**, 3146 (1995).

[29] M. Dijkstra and R. Evans, J. Chem. Phys. **112**, 1449 (2000).

[30] P. Tarazona, E. Chacón, and E. Velasco, Mol. Phys. **101**, 1595 (2003).

[31] It is interesting to remark that $\lim_{\beta\to\infty}\zeta(\rho,\beta) = 0$ if $\rho < (1 + \Delta/2)^{-1}$, while $\lim_{\beta\to\infty}\zeta(\rho,\beta) = \zeta_0(\rho) \neq 0$ if $\rho > (1 + \Delta/2)^{-1}$, where $\zeta_0(\rho)$ is the solution of $\rho^{-1} = \zeta_0^{-1} + (1 - \lambda e^{-\zeta_0\Delta})/(1 - e^{-\zeta_0\Delta})$.

[32] G. Zerah, J. Comput. Phys. **61**, 280 (1985).

[33] P. Perry and S. Fisk, J. Chem. Phys. **57**, 4065 (1972).

[34] R. J. Baxter, J. Chem. Phys. **49**, 2770 (1968).

[35] G. Stell, J. Stat. Phys. **63**, 1203 (1991).

[36] Y. Tago and S. Katsura, Can. J. Phys. **53**, 2587 (1975).

[37] N. A. Seaton and E. D. Glandt, J. Chem. Phys. **84**, 4595 (1986).